Atmos. Chem. Phys., 18, 2601–2614, 2018
https://doi.org/10.5194/acp-18-2601-2018

Atmospheric Chemistry and Physics
Open Access
EGU

Effects of temperature-dependent NO_x emissions on continental ozone production

Paul S. Romer[1], Kaitlin C. Duffey[1], Paul J. Wooldridge[1], Eric Edgerton[2], Karsten Baumann[2,3], Philip A. Feiner[4], David O. Miller[4], William H. Brune[4], Abigail R. Koss[5,6,7], Joost A. de Gouw[6,7], Pawel K. Misztal[8], Allen H. Goldstein[8,9], and Ronald C. Cohen[1,10]

[1]Department of Chemistry, University of California Berkeley, Berkeley, CA 94720, USA
[2]Atmospheric Research and Analysis Inc., Cary, NC 27513, USA
[3]Department of Environmental Sciences and Engineering, University of North Carolina at Chapel Hill, Chapel Hill, NC 27599, USA
[4]Department of Meteorology and Atmospheric Science, The Pennsylvania State University, University Park, PA 16802, USA
[5]Chemical Sciences Division, NOAA Earth System Research Laboratory (ESRL), Boulder, CO 80305, USA
[6]Cooperative Institute for Research in Environmental Sciences, University of Colorado Boulder, Boulder, CO 80309, USA
[7]Department of Chemistry and Biochemistry, University of Colorado Boulder, Boulder, CO 80309, USA
[8]Department of Environmental Science, Policy, and Management, University of California Berkeley, Berkeley, CA 94720, USA
[9]Department of Civil and Environmental Engineering, University of California Berkeley, Berkeley, CA 94720, USA
[10]Department of Earth and Planetary Sciences, University of California Berkeley, Berkeley, CA 94720, USA

Correspondence: Ronald C. Cohen (rccohen@berkeley.edu)

Received: 21 September 2017 – Discussion started: 25 September 2017
Revised: 11 January 2018 – Accepted: 15 January 2018 – Published: 22 February 2018

Abstract. Surface ozone concentrations are observed to increase with rising temperatures, but the mechanisms responsible for this effect in rural and remote continental regions remain uncertain. Better understanding of the effects of temperature on ozone is crucial to understanding global air quality and how it may be affected by climate change. We combine measurements from a focused ground campaign in summer 2013 with a long-term record from a forested site in the rural southeastern United States, to examine how daily average temperature affects ozone production. We find that changes to local chemistry are key drivers of increased ozone concentrations on hotter days, with integrated daily ozone production increasing by 2.3 ppb °C^{-1}. Nearly half of this increase is attributable to temperature-driven increases in emissions of nitrogen oxides (NO_x), most likely by soil microbes. The increase of soil NO_x emissions with temperature suggests that ozone will continue to increase with temperature in the future, even as direct anthropogenic NO_x emissions decrease dramatically. The links between temperature, soil NO_x, and ozone form a positive climate feedback.

1 Introduction

Elevated concentrations of tropospheric ozone are an important contributor to anthropogenic radiative forcing, and are associated with increased human mortality and decreased crop yields (Myhre et al., 2013; World Health Organization, 2005; Booker et al., 2009). Observations of increased surface ozone concentrations on hotter days are widely reported, but the mechanisms driving this relationship are poorly understood in regions and climates with low concentrations of nitrogen oxides ($NO_x \equiv NO + NO_2$). Understanding the mechanisms driving these increases is critical to effectively regulating ozone pollution and predicting the effects of global warming on air quality.

Several previous studies (e.g., Sillman and Samson, 1995; Weaver et al., 2009; Pusede et al., 2014) have used in situ observations and chemical transport models to examine the relationships between ozone (O_3) and temperature (T). Typically observed slopes range from 1 to 6 ppb °C^{-1}, with greater values occurring in more polluted environments (Pusede et al., 2015). A few studies have also reported that

this effect is nonlinear and can become significantly less strong at the highest temperatures (Steiner et al., 2010; Shen et al., 2016).

Increased ozone concentrations with temperature in urban areas can be well explained by increased ozone production caused by greater emissions of volatile organic compounds (VOCs) and decreased sequestration of NO_x in short-term reservoirs (Jacob and Winner, 2009). In contrast, there is little consensus on the mechanisms responsible for temperature-dependent changes in ozone concentrations in rural and remote environments. Arguments in favor of large-scale changes in atmospheric circulation and in favor of local changes in the chemical production and loss of ozone have both been presented (Barnes and Fiore, 2013; Steiner et al., 2006). Regional stagnation episodes, often associated with elevated temperatures, allow ozone to accumulate over several days and are known to contribute significantly to the ozone-temperature relationship (Jacob et al., 1993). How various temperature-dependent chemical effects interact and their relative contributions to ozone production are not well understood outside of polluted environments.

Summer daytime ozone concentrations at rural sites in the United States typically range from 35 to 55 ppb (Cooper et al., 2012), sufficient to cause harm to humans, crops, and the climate. Epidemiological studies and meta-analyses investigating the relationship between ozone and daily mortality have found significant effects in small cities and rural locations, with some studies suggesting that increases in ozone may have a greater effect on daily mortality under less polluted conditions (Vedal et al., 2003; Ito et al., 2005; Atkinson et al., 2012). Studies of crop yield and plant health have traditionally used a threshold of 40 ppb when investigating the effects of ozone exposure, but many crops have been shown to experience reduced yields when exposed to ozone concentrations as low as 20 ppb (Pleijel et al., 2004; Booker et al., 2009). From a regulatory perspective, elevated regional background ozone can strongly exacerbate ozone pollution and the probability of regulatory exceedances in urban areas such as Houston (Berlin et al., 2013). Understanding the behavior of O_3 in the rural and remote areas that cover the majority of the land area of the Earth is therefore crucial for effectively predicting and controlling air quality now, and in the future.

In this paper we use observations from Centreville, Alabama (CTR), a rural site in the southeastern United States (Supplement Fig. S1), to investigate how temperature affects ozone production. Long-term monitoring from the South-Eastern Aerosol Research and CHaracterization (SEARCH) network shows that ozone increases significantly with temperature at this site (Fig. 1), despite being in a low-NO_x environment where the predicted response of the instantaneous ozone production rate to temperature is small (Pusede et al., 2015). We combine this record with extensive measurements from the Southern Oxidant and Aerosol Study (SOAS) in summer 2013 to explicitly calculate daily integrated ozone production and NO_x loss as a function of daily average temperature. We find that changes in local chemistry are important drivers of the increase in ozone concentrations observed at this site, and that increased NO_x emissions are responsible for 40 % of the temperature-dependent increase in daily integrated ozone production. We expect similar effects to be present in other low-NO_x areas with high concentrations of VOCs, where the chemistry of alkyl and multifunctional nitrates is the majority pathway for permanent NO_x loss.

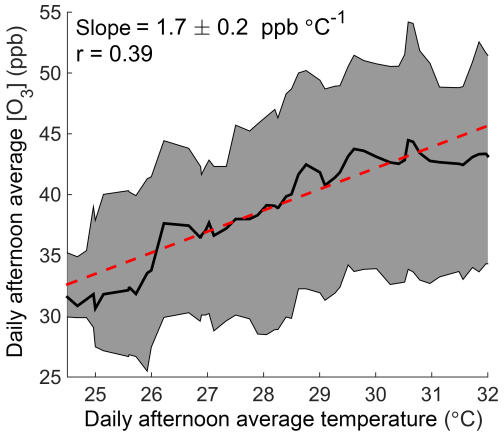

Figure 1. The O_3–temperature relationship in Centreville, Alabama. Daily afternoon (12:00–16:00) average ozone concentration is shown as a function of temperature over June–August 2010–2014 at the SEARCH CTR site. The black line and shaded gray region show the running median and interquartile range of ozone with temperature, respectively. The red line represents a fit to all daily data points.

2 Chemistry of ozone production and predicted response to temperature

Observed O_3–T relationships are caused by a combination of chemical changes to the production and loss of O_3 and changes to atmospheric circulation that determine advection and mixing. To begin separating these effects, we consider the chemical production of ozone (PO_3) and how it changes with temperature. Temperature-dependent changes in ozone production may be driven directly by temperature, or by another meteorological parameter that co-varies with temperature, such as solar radiation.

Ozone is produced in the troposphere when NO is converted to NO_2 by reaction with HO_2 or RO_2 in the linked HO_x and NO_x cycles (Fig. 2a). HO_2 and RO_2 radicals are generated in the HO_x cycle when a VOC reacts with OH in the presence of NO_x. In one turn of the cycle, the VOC is oxidized, OH is regenerated, and two molecules of O_3 are formed. The reactions that drive these catalytic cycles forward are in constant competition with reactions that remove radicals from the atmosphere, terminating the cycles. Termination can occur either through the association of two HO_x

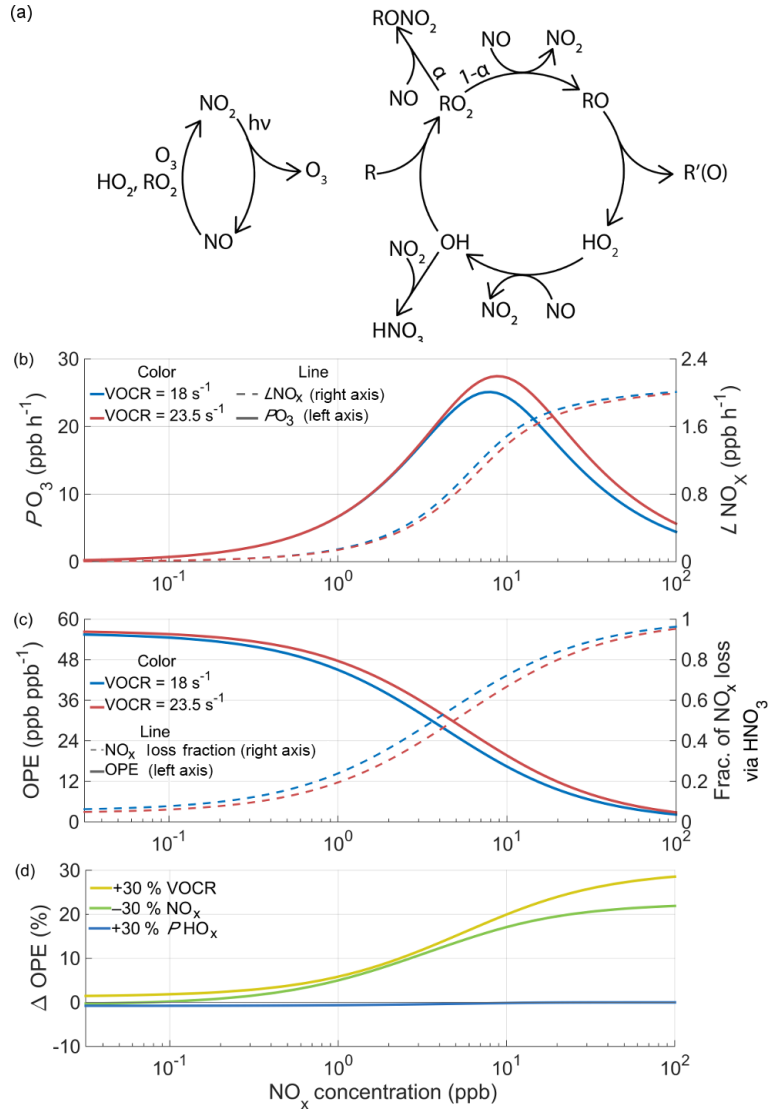

Figure 2. The chemistry of ozone production and NO_x loss in the troposphere. **(a)** Schematic of the linked NO_x and HO_x cycles that lead to net ozone production. **(b)** The calculated instantaneous O_3 production rate and NO_x loss rate as a function of NO_x and VOCR, with fixed PHO_x, η, and α_{eff}. **(c)** OPE and the fraction of NO_x loss that takes place via HNO_3 chemistry under the same conditions as **(b)**. **(d)** The percent change in ozone production efficiency caused by chemical changes as a function of NO_x.

radicals to form inorganic or organic peroxides, or through the association of HO_x and NO_x radicals to form nitric acid or an organic nitrate.

The balance between propagating and terminating reactions causes PO_3 to be a non-linear function of the NO_x and VOC reactivity (VOCR), as well as the production rate of HO_x radicals (PHO_x). The largest source of HO_x radicals in the summertime is the photolysis of O_3 followed by reaction with water vapor to produce OH; additional sources include the photolysis of formaldehyde and peroxides, ozonolysis of alkenes, and isomerization pathways in the oxidation of isoprene and other VOCs. To understand the response of ozone production to changes in chemistry, we use a simplified framework based on the balance of HO_x radical production and loss (Farmer et al., 2011).

Under moderate or high NO_x conditions, the primary loss process of HO_2 and RO_2 radicals is reaction with NO, and the concentration of OH radicals can be expressed as a quadratic equation. To modify this approach to work under low-NO_x conditions, reactions between HO_x radicals must also be included, leading to a set of four algebraic equations that can be solved numerically (details given in Appendix A). Figure 2b shows the calculated rate of ozone production as a function of NO_x at two different VOC reactivities. Depending on atmospheric conditions, the ozone production rate can either be NO_x-limited, where additional NO_x causes PO_3 to increase,

or NO_x-saturated, where additional NO_x suppresses ozone formation.

When considering day-to-day variations, the total amount of ozone produced over the course of a day ($\int PO_3$) is a more representative metric than the instantaneous ozone production rate. Total daily ozone production depends on all of the factors that affect PO_3 as well as their diurnal evolution. In places where ozone production is NO_x-limited, changes to chemistry with temperature that affect the NO_x loss rate ($\mathcal{L}NO_x$) can affect $\int PO_3$ by changing the amount of NO_x available for photochemistry later in the day (Hirsch et al., 1996).

Permanent NO_x loss occurs through two primary pathways in the troposphere: the association of OH and NO_2 to form HNO_3, and through the chemistry of alkyl and multifunctional nitrates ($\Sigma RONO_2$). These organic nitrates are formed as a minor channel of the $RO_2 + NO$ reaction, with the alkyl nitrate branching ratio α_i ranging from near zero for small hydrocarbons to over 0.20 for monoterpenes and long-chain alkanes (Perring et al., 2013). The overall alkyl nitrate branching ratio α_{eff} represents the reactivity-weighted average of α_i for all VOCs. While some fraction of $\Sigma RONO_2$ quickly recycles NO_x to the atmosphere, a significant fraction η permanently removes NO_x through deposition and hydrolysis (e.g., Browne et al., 2013). Romer et al. (2016) determined that $\eta = 0.55$ during SOAS and was controlled primarily by the hydrolysis of isoprene hydroxy-nitrates. Because the hydrolysis rate is set primarily by the distribution of nitrate isomers, which does not change appreciably with temperature, we assume that η is constant with temperature in this study (Hu et al., 2011; Peeters et al., 2014). Deposition is only a minor loss process for $\Sigma RONO_2$, therefore any changes in the deposition rate with temperature will have, at most, a minor effect on η.

NO_x also has several temporary sinks that can sequester NO_x, most importantly peroxy acyl nitrate (PAN). In the summertime in the southeastern United States, the lifetime of PAN is typically 1–2 h, too short to act as a permanent sink of NO_x. Past studies in forested regions have found remarkably little variation in PAN with temperature, due to compensating changes in both its production and loss (e.g., LaFranchi et al., 2009). As a result, the formation or destruction of PAN does not contribute significantly to net ozone production or NO_x loss and we do not include it in these calculations.

The ozone production efficiency (OPE $\equiv PO_3/\mathcal{L}NO_x$) represents the number of ozone molecules formed per molecule of NO_x consumed and directly links the ozone and NO_x budgets. Because OPE accounts for changes in both PO_3 and $\mathcal{L}NO_x$, the temperature response of OPE captures feedbacks in ozone production chemistry that PO_3 alone does not.

As the concentration of NO_x decreases and VOCR increases, the fraction of NO_x loss that takes place via HNO_3 chemistry decreases and the OPE increases (Fig. 2c). The relative importance of HNO_3 and $RONO_2$ chemistry determines the relationship between PO_3 and $\mathcal{L}NO_x$. When HNO_3 is the most important NO_x loss pathway, O_3 production and NO_x loss occur through separate channels. O_3 production occurs when OH reacts with a VOC, generating RO_2 and HO_2 radicals; NO_x loss primarily occurs when OH reacts with NO_2. Although these channels are linked by a shared dependence on OH, the relative importance of these pathways can vary. For example, under these conditions an increase in VOCR will cause NO_x loss to decrease, ozone production to increase, and OPE to increase (Fig. 2b–c).

In contrast, when $RONO_2$ chemistry dominates NO_x loss, ozone production and NO_x loss are intrinsically linked by their shared dependence on the $RO_2 + NO$ reaction. This reaction produces O_3 in its main channel and consumes NO_x in the minor channel that forms organic nitrates, with the ratio between these two channels set by α_{eff}. Under these conditions, changes to the chemistry that do not affect α_{eff} have a minimal effect on OPE (Fig. 2d) and the OPE can be considered to be unvarying with temperature. An increase in VOCR or a decrease in NO_x will affect both NO_x loss and ozone production equally, because both processes are dependent on the same set of reactions. Because of this change in behavior, from variable OPE to fixed OPE, the drivers of the O_3–T relationship are expected to be categorically different in areas where $RONO_2$ chemistry dominates NO_x loss. As a result, the effects that cause O_3 to increase with temperature in urban and other polluted regions, where HNO_3 chemistry dominates NO_x loss, are unlikely to apply in areas with low concentrations of NO_x and high concentrations of reactive VOCs, where $RONO_2$ chemistry is most important. In these areas, more NO_x must be oxidized in order to produce more O_3.

3 Observed response of ozone production to temperature

3.1 Measurements during SOAS

The theoretical results presented in Fig. 2 can be compared to the observed behavior during SOAS (SOAS Science Team, 2013). Measurements during SOAS have been described in detail elsewhere (e.g., Hidy et al., 2014; Romer et al., 2016; Feiner et al., 2016) and are summarized below. The primary ground site for SOAS was co-located with the CTR site of the SEARCH network (32.90289° N, 87.24968° W), in a clearing surrounded by a dense mixed forest (Hansen et al., 2003). Direct anthropogenic emissions of NO_x near this site are estimated to be low and predominantly from mobile sources (Hidy et al., 2014). Figure S1 shows the location of the CTR site relative to major population centers in the region. Measurements taken as part of the SEARCH network were located on a 10 m tower approximately 100 m away from the forest edge, while the other measurements from the SOAS campaign used in this analysis were located on a 20 m walk-

up tower at the edge of the forest. Species measured on both the SOAS walk-up tower and the SEARCH platform were well correlated with each other, indicating that similar air masses were sampled at both locations.

Several chemical and meteorological measurements used in this study, including NO_x, O_3, total reactive nitrogen (NO_y), and temperature, were collected by Atmospheric Research and Analysis (ARA) as part of SEARCH (Hidy et al., 2014). NO was measured using the chemiluminescent reaction of NO with excess ozone. NO_2 was measured based on the same principle, using blue LED photolysis to convert NO_2 to NO. The photolytic conversion of NO_2 to NO is nearly 100 % efficient and does not affect higher oxides of nitrogen (Ryerson et al., 2000). Ozone was measured using a commercially available ozone analyzer (Thermo-Scientific 49i).

During the SOAS campaign, NO_2, total peroxy nitrates (ΣPNs), and total alkyl and multifunctional nitrates ($\Sigma RONO_2$) were measured via thermal dissociation laser-induced fluorescence, as described by Day et al. (2002). An NO chemiluminescence instrument located on the walk-up tower provided additional measurements of NO co-located with the other SOAS measurements (Min et al., 2014).

HO_x radicals were measured with the Penn State Ground-based Tropospheric Hydrogen Oxides Sensor (GTHOS), which uses laser-induced fluorescence to measure OH (Faloona et al., 2004). HO_2 was also measured in this instrument by adding NO to convert HO_2 to OH. C_3F_6 was periodically added to the sampling inlet to quantify the interference from internally generated OH (Feiner et al., 2016). Measurements of total OH reactivity (OHR $\equiv$ inverse OH lifetime) were made by sampling ambient air, injecting OH, and letting the mixture react for a variable period of time. The slope of the OH signal vs. reaction time provides a top-down measure of OHR (Mao et al., 2009).

A wide range of VOCs were measured during SOAS using gas chromatography-mass spectrometry (GC-MS). Samples were collected in a liquid-nitrogen cooled trap for five minutes, then transferred by heating onto an analytical column, and detected using an electron-impact quadrupole mass-spectrometer (Gilman et al., 2010). This system is able to quantify a wide range of compounds including alkanes, alkenes, aromatics, isoprene, and multiple monoterpenes at a time resolution of 30 min. Methyl vinyl ketone (MVK) and methacrolein (MACR) were measured individually by GC-MS and their sum was also measured using a proton transfer reaction mass spectrometer (PTR-MS) (Kaser et al., 2013). The calculated rates of ozone production and NO_x loss do not change significantly depending on which measurement is used.

3.2 Calculation of $\int PO_3$ and effects of temperature

During the SOAS campaign, afternoon concentrations of NO_x averaged 0.3 ppb and concentrations of isoprene 5.5 ppb

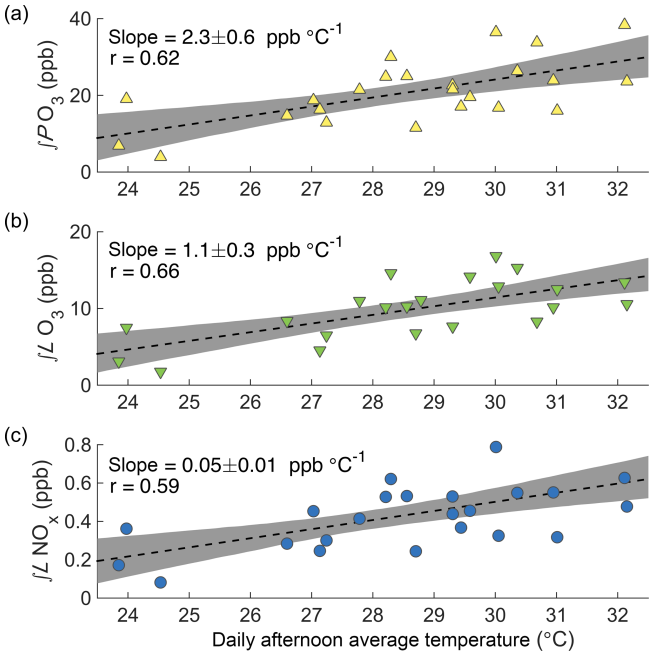

Figure 3. Observed dependence of daily $\int PO_3$ **(a)**, $\int \mathcal{L}O_3$ **(b)**, and $\int \mathcal{L}NO_x$ **(c)** on daily afternoon average temperature during SOAS. Each point shows the afternoon average temperature and integrated production or loss for a single day. Black lines show a least squares fit to all points; shaded areas show the 90 % confidence limits of the fit calculated via bootstrap sampling.

(Fig. S2). $\Sigma RONO_2$ chemistry was responsible for over three-quarters of the permanent NO_x loss (Romer et al., 2016). Daily average afternoon (12:00–16:00) ozone concentrations increased with daily average afternoon temperature during SOAS (2.3 ± 1 ppb °C^{-1}). This trend is greater than the long-term trend reported by the SEARCH network, but the difference is not statistically significant.

Measurements of NO, NO_2, OH, HO_2, and a wide range of VOCs (Table S1) were used to calculate the steady-state concentrations of RO_2 radicals using the Master Chemical Mechanism v3.3.1, run in a MATLAB framework (Jenkin et al., 2015; Wolfe et al., 2016). Before 24 June, HO_2 measurements are not available and steady-state concentrations of both HO_2 and RO_2 were calculated. Input species were taken to 30 min averages, and the model was run until radical concentrations reached steady state. Top-down measurements of OHR were used to include the contribution to ozone production from unmeasured VOCs.

To understand the day-to-day variation of ozone chemistry, the calculated ozone production rate was integrated from 06:00 to 16:00 for each of the 24 days during the campaign period with greater than 75 % data coverage of all input species. When plotted against daily average afternoon temperature, $\int PO_3$ is seen to increase strongly with temperature (2.3 ± 0.6 ppb °C^{-1}, Fig. 3a). The change in $\int PO_3$ with temperature demonstrates that local chemistry is an impor-

tant contributor to the observed O_3–T relationship; however, the observed O_3–T trend also includes the effects of chemical loss, advection, entrainment, and multi-day buildup on overall O_3 concentration (e.g., Baumann et al., 2000).

While elevated temperatures are associated with enhanced production of ozone, they are also associated with increased chemical loss. The chemical loss of ozone occurs via three main pathways in this region: photolysis followed by reaction with H_2O, reaction with HO_2, and reaction with VOCs (Frost et al., 1998). The loss of O_3 was calculated for each of these pathways, and then integrated over the course of the day to determine total daily ozone loss ($\int \mathcal{L}O_3$). Chemical loss of ozone is found to increase with temperature ($1.1 \pm 0.3\,\mathrm{ppb\,°C^{-1}}$, Fig. 3b), but much less than the chemical production.

The difference between the trend in the net chemical production and loss of O_3 and the trend in ozone concentration gives a rough estimate of how non-chemical processes contribute to the ozone–temperature relationship. We calculate that non-chemical processes cause O_3 to increase by $1 \pm 1.2\,\mathrm{ppb\,°C^{-1}}$. This approach does not take into account the interactions between chemical and non-chemical effects, such as how changes to advection and mixing may impact concentrations of VOCs, NO_x, and other reactants. Although the large uncertainty does not allow for quantitative analysis, qualitatively, chemical and non-chemical processes are both found to be important contributors to the ozone–temperature relationship. Other approaches, such as chemical transport models, that can more directly investigate and control specific physical processes are likely to be better suited to calculating the contribution of non-chemical processes to the ozone–temperature relationship (e.g., Fu et al., 2015).

Using the same calculated radical concentrations, the rate of NO_x loss was calculated as the rate of direct HNO_3 production plus the fraction η of alkyl nitrate production that leads to permanent NO_x loss. Figure 3c shows the increase in $\int \mathcal{L}NO_x$ with temperature for the SOAS campaign ($0.05 \pm 0.01\,\mathrm{ppb\,°C^{-1}}$). As expected from the importance of $RONO_2$ chemistry to NO_x loss, $\int \mathcal{L}NO_x$ and $\int PO_3$ are tightly correlated ($r^2 = 0.90$), and OPE is high (OPE average $45 \pm 3\,\mathrm{ppb\,ppb^{-1}}$) and is effectively constant with temperature (calculated trend $0.2 \pm 0.6\,\mathrm{°C^{-1}}$). Therefore, the increase in $\int PO_3$ with temperature is not caused by more efficient production of ozone while the same amount of NO_x is consumed.

OPE can also be estimated from the ratio of odd oxygen ($O_x \equiv O_3 + NO_2$) to NO_x oxidation products ($NO_z \equiv NO_y - NO_x$) (Trainer et al., 1993). The afternoon ratio of O_x to NO_z during SOAS varied from 43 to 67 (interquartile range), slightly higher than the average ratio of $\int PO_3$ to $\int \mathcal{L}NO_x$. However, since the O_x to NO_z ratio includes the effects of chemical loss and transport, which the ratio of $\int PO_3$ to $\int \mathcal{L}NO_x$ does not, these two values are not expected to be equivalent, particularly in non-polluted areas.

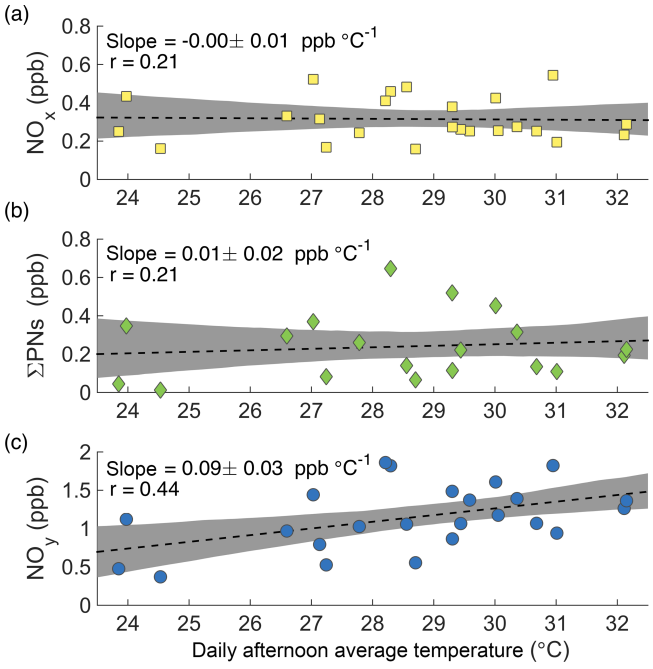

Figure 4. Afternoon average concentrations of NO_x **(a)**, ΣPNs **(b)**, and NO_y **(c)** at the CTR site as a function of daily average afternoon temperature during SOAS.

The trend in $\int PO_3$ with temperature is robust and extends beyond the short temporal window of the SOAS campaign. Although long-term measurements of HO_x and VOCs are not available, the ozone production rate can be estimated from SEARCH measurements using the deviation of NO and NO_2 from photostationary state (Eq. 1) (Baumann et al., 2000; Pusede et al., 2015).

$$PO_3 = j_{NO_2}[NO_2] - k_{NO+O_3}[NO][O_3] \quad (1)$$

The NO_2 photolysis rate was parameterized as a quadratic function of total solar radiation (Trebs et al., 2009). Using this method and scaling the result to match the values calculated using steady-state RO_2 concentrations during SOAS, we find that $\int PO_3$ increased by $2.3 \pm 0.8\,\mathrm{ppb\,°C^{-1}}$ during June–August 2010–2014 (Fig. S3). Without scaling, the long-term trend in $\int PO_3$ with temperature is $4.0 \pm 0.5\,\mathrm{ppb\,°C^{-1}}$. Based on the long-term SEARCH record, we do not find evidence that the relationship between temperature and ozone concentration or ozone production changes significantly at the highest temperatures (the top 5 % of observations). This agrees broadly with Shen et al. (2016), who found ozone suppression at extreme temperatures to be uncommon in the southeastern United States.

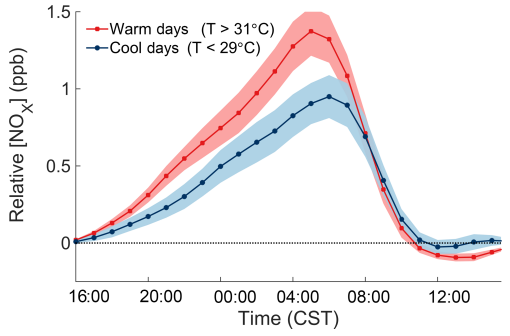

Figure 5. Concentrations of NO_x relative to their concentration at 16:00 the day before over June–August 2010–2014 at the CTR site. The thick lines and shaded areas show the hourly mean and 90 % confidence interval of the mean for cool and warm days.

4 Drivers of increased ozone production

While the increase in ozone production is accompanied by an observed increase in ozone concentration, the increase in NO_x loss is not accompanied by a significant decrease in NO_x concentration (-0.002 ± 0.01 ppb °C^{-1}, Fig. 4a). For this to occur, NO_x must have a source that increases with temperature to compensate for its increased loss. One possible explanation is that the increased thermal decomposition rate of peroxy nitrates (ΣPNs) causes less NO_x to be sequestered in these short-term reservoirs. This is not the case during SOAS. The increased decomposition rate of peroxy nitrates is counteracted by an increase in their production rate, such that the average concentration of total peroxy nitrates shows no decrease with temperature (Fig. 4b).

More generally, increased transformations from NO_x oxidation products back into NO_x cannot explain the observations. The concentration of NO_y increases significantly with temperature (Fig. 4c). Because NO_y includes NO_x as well as all of its reservoirs and sinks, changes in the transformation rates between NO_x and its oxidation products cannot explain the increase of NO_y with temperature. There must be a source of NO_y, not just of NO_x, that increases with temperature.

Data from the SEARCH network indicate that the increase in NO_y with temperature observed during SOAS is primarily a local effect. Measurements from June to August 2010–2014 show a consistent increase of NO_y with temperature at the two rural monitoring sites in the network, but total NO_y decreases with temperature at the four urban and suburban sites (Table S2). The increase in NO_y with temperature cannot therefore be explained by regional meteorological effects, since those would lead to similar relationships between NO_y and temperature across the southeastern United States.

Measurements at night and in the early morning, before significant photochemistry has occurred, show a strong temperature-dependent increase of NO_x over the course of the night. Because surface wind speeds are low at night and the increase in NO_x during the night is not accompanied by large increases in NO_x oxidation products, the increase in NO_x must be caused by emissions local to the CTR site.

The consistent increase of NO_x over the course of the night can be used to quantitatively measure the local NO_x emissions rate. Figure 5 shows the temperature-dependent increase of NO_x relative to the concentration of NO_x at 16:00 the day before, separating the effects of the previous day from the nighttime increase. Measurements from June to August 2010–2014 from the CTR SEARCH network site are used to obtain more representative statistics. The average rate of NO_x increase during the night is 0.095 ppb h^{-1}. To account for the chemical removal of NO_x, the cumulative loss of NO_x during the night was added to the observations. During SOAS, the nighttime loss of NO_x occurred almost exclusively through the reaction of NO_2 with O_3 to form NO_3, which then reacted with a VOC to form an organic nitrate (Ayres et al., 2015). N_2O_5 chemistry made a negligible contribution to total NO_x loss. The loss rate of NO_x during the night was therefore calculated as the rate of reaction of NO_2 with O_3. In this form, the rate of increase of the adjusted NO_x concentrations (NO_x^*) is equal to the local NO_x emission rate. The emission rate of NO_x and its temperature dependence were calculated by a linear regression following the form of Eq. (2), where the adjusted concentration of NO_x depends both on time (H is hours after 16:00) and temperature (T).

$$NO_x^* = (\alpha T + \beta)H + b \quad (2)$$

In this regression, the fitted parameter α represents the increase of NO_x emissions with temperature and the average value of $\alpha T + \beta$ provides an estimated NO_x emission rate.

Because emissions are localized to the surface, the effective depth of the nighttime boundary layer must also be accounted for, which we estimate to be 150 m. This agrees well with the derived mixing heights from daily 05:00 sonde launches at the Birmingham (BHM) airport (Durre and Yin, 2008) and past estimates of the nocturnal boundary layer height (e.g., Liu and Liang, 2010; VandenBoer et al., 2013), while it is significantly lower than the average ceilometer-reported 05:00 boundary layer height of 400 m during SOAS (Fig. S4).

After accounting for these factors, the NO_x emissions rate is calculated to be 7.4 ppt m s^{-1} or 4.2 ng N m^{-2} s^{-1}. Based on the change in slope with temperature, the emissions rate is estimated to increase by 0.4 ppt m s^{-1} °C^{-1}. The rise in NO_x emissions with temperature over 24 h agrees to within the uncertainty with the increase of daily $\int \mathcal{L}NO_x$ with temperature, sufficient to explain why afternoon NO_x concentrations are not observed to decrease with temperature even as their loss rate increases.

The inferred local NO_x source bears all the hallmarks of soil microbial emissions (S_{NO_x}). Soil microbes emit NO_x as a byproduct of both nitrification and denitrification, and the rate of NO_x emissions strongly correlates with microbial activity in soil (Pilegaard, 2013). The inferred NO_x source is

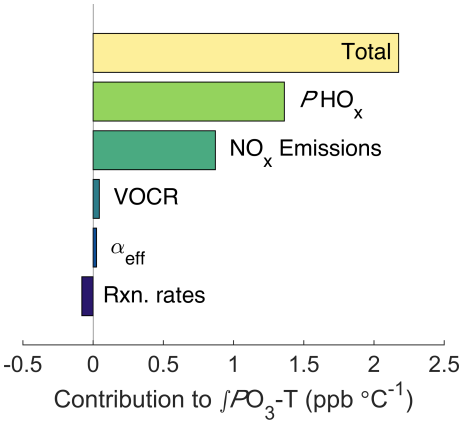

Figure 6. Decomposed effects of ozone and temperature. The top bar shows the model-calculated $\int P\mathrm{O_3}$-T trend, all other bars show how the $\int P\mathrm{O_3}$-T slope changes when the temperature dependence of each factor is removed.

active during day and night, increases strongly with temperature, and is present in a rural area with low anthropogenic emissions. The only plausible source of NO_x that matches all of these constraints is soil microbial emissions near the SOAS site. Soil NO_x emissions also depend on the water content and nitrogen availability, neither of which is generally limiting in the southeastern United States (e.g., Hickman et al., 2010). The most likely anthropogenic sources of NO_x at this location are mobile sources, which are not thought to change significantly with temperature (Singh and Sloan, 2006) , and therefore cannot explain the results of Fig. 5.

To calculate how the increase in NO_x emissions affects ozone production, we use the same chemical framework from Fig. 2. For each half-hour period the average value of the input parameters and their temperature dependence during the SOAS campaign were calculated (Fig. S5). The diurnal cycle and trend with temperature of all model inputs were then used to calculate total daily ozone production as a function of temperature (Fig. S6). By altering whether the temperature dependence for each parameter is included, the overall trend in $\int P\mathrm{O_3}$ can be decomposed into individual components (Fig. 6). The effect of increased NO_x emissions was calculated by fixing the trend in NO_x with temperature to match the trend in $\int \mathcal{L}\mathrm{NO_x}$. We find that the increase of NO_x emissions with temperature accounts for 40 % of the increase in $\int P\mathrm{O_3}$ with temperature, or approximately 0.9 ppb °C^{-1}. The other 60 % is primarily caused by the increase of $P\mathrm{HO_x}$ with temperature. The increase in $P\mathrm{HO_x}$ with temperature is most likely caused by changes in solar radiation, which is well correlated with the total $P\mathrm{HO_x}$ rate (Fig. S7a) and increases strongly with temperature. In contrast, water vapor is not correlated with total $P\mathrm{HO_x}$ (Fig. S7b). Although VOCR increases strongly with temperature, the $\mathrm{RONO_2}$-dominated NO_x chemistry causes neither the ozone production rate nor the NO_x loss rate to be sensitive to this increase, leading to the minimal effect of VOCR on $\int P\mathrm{O_3}$.

5 Conclusions

Changes in NO_x emissions with temperature have an outsized effect when considering the impacts of ozone on human health and climate. At the CTR site and other areas where OPE does not vary with temperature, the total amount of ozone produced on weekly or monthly timescales is directly proportional to the amount of available NO_x. While faster oxidation on hotter days causes more ozone to be produced, without changes in NO_x emissions there would be an associated decrease in ozone production on subsequent days, because the NO_x necessary for ozone production would be depleted. In contrast, increased NO_x emissions can cause weekly or monthly average ozone concentrations to increase with temperature. Change in long-term average ozone concentrations is often more important to the ozone climate feedback and human health than day-to-day variation. The mechanisms described here are likely to be active in all areas with low concentrations of NO_x and high concentrations of reactive VOCs. Only regions where $\mathrm{RONO_2}$ chemistry is the dominant pathway for NO_x loss have effectively constant OPE with temperature, but the effect of soil NO_x emissions on ozone production is widespread.

Past direct measurements of soil NO_x using soil chambers have found enormous variability, both between sites and within different plots in the same field. Pilegaard et al. (2006) found variability of a factor of over 100 between soil NO_x emissions in different European forests. Within the southeastern United States, direct measurements at forested sites have reported emissions rates ranging from 0.1 to 10 ng N $\mathrm{m^{-2}\,s^{-1}}$ (Williams and Fehsenfeld, 1991; Thornton et al., 1997; Hickman et al., 2010). Besides temperature, the most important variables affecting soil NO_x emissions are typically nitrogen availability and soil water content, as well as plant cover and soil pH (Pilegaard, 2013). In very wet environments, soil microbes typically emit N_2O or N_2 instead of NO_x, and in arid environments soil emissions of HONO can be equal to or larger than soil NO_x emissions (Oswald et al., 2013). Although conditions at the CTR site are too wet and acidic for soil HONO emissions to be significant, in environments where soil HONO emissions are large, they would likely have an even greater effect on ozone production by acting as a source of both NO_x and HO_x radicals.

The variability between sites and the interaction between several biotic and abiotic factors make it difficult to apply regional or model estimates of soil NO_x emissions to a particular location. Our approach from this study, using observations of the nighttime atmosphere to determine the NO_x emissions rate, helps span the gap between soil chambers and the regional atmosphere. Although soil NO_x emissions depend on several environmental factors, process-driven mod-

els predict that the response of soil NO_x emissions to global warming will be driven primarily by the increase in temperature (Kesik et al., 2006).

While soil NO_x emissions have been known and studied for decades, the impact of soil NO_x emissions on ozone from non-agricultural regions was often found to be insignificant compared to anthropogenic sources (e.g., Davidson et al., 1998). Years of declining anthropogenic NO_x emissions in the United States and recent higher estimates for forest soil NO_x emissions (e.g., Hickman et al., 2010) mean that this is no longer the case. Non-agricultural soil NO_x emissions may now account for nearly a third of total NO_x emissions in the summertime in the southeastern United States (Travis et al., 2016), and have significant effects on regional ozone production.

The rise in ozone production caused by increased NO_x emissions on hotter days established here suggests that the relationship between ozone and temperature will be positive under a wider range of conditions than previously thought. This includes 1. the pre-industrial atmosphere, 2. present day rural continental locations, and 3. future scenarios with dramatically reduced anthropogenic NO_x emissions.

1. In pre-industrial times, semi-quantitative measurements of ozone show significantly lower concentrations of ozone than are currently observed in rural and remote regions or generally predicted by global models (Cooper et al., 2014). While alkyl nitrate chemistry establishes an upper limit to the ozone production efficiency under low-NO_x conditions, the significant contribution of S_{NO_x} to ozone production makes reconciling the semi-quantitative measurements with model predictions more difficult and suggests that natural emissions of NO_x in pre-industrial models may be over-estimated (Mickley et al., 2001).

1. In the present day, effective ozone regulation, especially on hot days, requires taking the effect of S_{NO_x} into account. Because these emissions are distributed over broad areas and are not directly anthropogenic, they present additional challenges to air quality management. Indirect approaches, such as changes to fertilizer application practices, have the potential to significantly reduce S_{NO_x} from agricultural regions (Oikawa et al., 2015). Decreases in direct anthropogenic NO_x emissions may also lead to a decrease in S_{NO_x} by reducing the amount of nitrogen available to the ecosystem (Pilegaard, 2013).

2. In the future, because soil NO_x emissions lead to the formation of ozone, itself an important greenhouse gas, the increase of soil NO_x emissions with temperature represents a positive climate feedback and an additional link between changes to the nitrogen cycle and the environment. The effects of increased ozone pollution to plants, including reduced photosynthesis and slower growth, have the potential to alter the carbon cycle on a regional scale (Heagle, 1989; Booker et al., 2009). Soil NO_x emissions therefore represent an additional link between the nitrogen and carbon cycles that should be included when considering the consequences of a warming world.

Data availability. Measurements from the SOAS campaign are available at https://esrl.noaa.gov/csd/groups/csd7/measurements/2013senex/Ground/DataDownload (SOAS Science Team, 2013).

Appendix A

A1 Analytical PO_3 model

To conceptually understand O_3 production and NO_x loss, we use a simplified framework similar to that described by Farmer et al. (2011). This framework uses fixed values of total organic reactivity (VOCR), alkyl nitrate branching ratio α and loss efficiency η, NO_x, and HO_x radical production rate (PHO_x).

Since HO_x radicals are highly reactive, it is a valid assumption under nearly all NO_x concentrations that HO_x radicals are in steady state and that PHO_x is equal to the gross HO_x loss rate (Eq. A1).

$$\begin{aligned} PHO_x &= k_{OH+NO_2}[OH][NO_2] \\ &+ \alpha \cdot k_{RO_2+NO}[RO_2][NO] + 2k_{HO_2+HO_2}[HO_2][HO_2] \\ &+ 2k_{RO_2+HO_2}[RO_2][HO_2] + 2k_{RO_2+RO_2}[RO_2][RO_2] \end{aligned} \quad (A1)$$

Individual HO_x radicals (OH, HO_2, and RO_2) can also be assumed to be in steady state, such that their production and loss are equal. Under low-NO_x conditions, the reactions that initiate and terminate the HO_x cycle must be included, as well as the cycling rate. We further constrain the model by requiring that the concentration of HO_2 and RO_2 radicals be equal. This constraint is satisfied by introducing an additional parameter c which allows PHO_x to produce both HO_2 and OH radicals in a varying ratio. These constraints provide a system of four equations that can be solved numerically (Eqs. A2–A5).

$$[OH] = \frac{k_{HO_2+NO}[HO_2][NO] + c \cdot PHO_x}{VOCR + k_{OH+NO_2}[NO_2]} \quad (A2)$$

$$[RO_2] = \frac{[OH] \cdot VOCR}{k_{RO_2+NO}[NO] + k_{RO_2+HO_2}[HO_2] + 2k_{RO_2+RO_2}[RO_2]} \quad (A3)$$

$$[HO_2] = \frac{(1-\alpha)k_{RO_2+NO}[RO_2][NO] + (1-c)PHO_x}{k_{HO_2+NO}[NO] + 2k_{HO_2+HO_2}[HO_2] + k_{HO_2+RO_2}[RO_2]} \quad (A4)$$

$$[HO_2] = [RO_2] \quad (A5)$$

For the calculations in Fig. 2, the values of VOCR, α, and PHO_x were fixed at 18 s^{-1}, 0.06, and 1.15×10^7 molec cm^{-3} s^{-1}. Rate constants are taken from the IUPAC chemical kinetics database, assuming that all RO_2 radicals react with the kinetics of $CH_3CH_2O_2$ (Atkinson et al., 2006). The system of equations was solved numerically using the `vpasolve` function in MATLAB, subject to the constraints that [OH],[HO_2], and [RO_2] are positive and c is between 0 and 1.

The resulting concentrations of HO_x radicals can be used to calculate the rates of ozone production and NO_x loss using Eqs. (A6)–(A9).

$$PO_3 = (1-\alpha)k_{RO_2+NO}[RO_2][NO] + k_{HO_2+NO}[HO_2][NO] \quad (A6)$$

$$PHNO_3 = k_{OH+NO_2}[OH][NO_2] \quad (A7)$$

$$P\Sigma RONO_2 = \alpha \cdot k_{RO_2+NO}[RO_2][NO] \quad (A8)$$

$$LNOx = PHNO_3 + \eta \cdot P\Sigma RONO_2 \quad (A9)$$

A2 Decomposition of the O_3-temperature relationship

The simplified HO_x model described above was used to decompose the contribution of different parameters to the increase of $\int PO_3$ with temperature. Peroxy nitrates are not included in this model, but because there is no significant trend in ΣPNs with temperature their absence does not affect the results. To validate that this model gave accurate $\int PO_3$ results, it was first run using inputs based on measured values for each half-hour period:

- Model inputs of NO_x were taken directly from measurements of NO and NO_2
- VOCR was calculated as the measured OHR minus the reactivity of species that do not form RO_2 radicals (e.g., CO, NO_2)
- PHO_x was calculated as equal to the measured rate of HO_x loss, using Eq. (A1) and measured HO_x radical concentrations
- α_{eff} was calculated as the reactivity-weighted average of α_i for all measured VOCs.

The comparison of $\int PO_3$ calculated from the full data set and that from the steady-state HO_x model is shown in Fig. S6a. The two calculations are well-correlated with a slope close to one, showing that the steady-state HO_x model can accurately reproduce ozone production at this location.

To use this model to explore how ozone production changes with temperature, the diurnal cycle and trend in temperature of each of these inputs was calculated. Because the response to temperature is different at different times of day, the trend with temperature was calculated independently for each half-hour bin, and is shown in Fig. S5. These trends were used to construct temperature-dependent diurnal cycles of each of the parameters, which were then used as inputs to the model at a range of daily average afternoon temperatures from 24 to 32 °C. Figure S6b shows that $\int PO_3$ calculated this way has a very similar trend with temperature as that using the full data set, although it cannot capture day-to-day variability not caused by temperature. The nonlinear shape of the trend with temperature is caused primarily by the imposed exponential increase of PHO_x with temperature. Using a linear or quadratic increase of PHO_x with temperature changes the shape of the increase but does not significantly affect the overall $\int PO_3$-T slope.

Competing interests. The authors declare that they have no conflict of interest.

Supplement. The supplement related to this article is available online at: https://doi.org/10.5194/acp-18-2601-2018-supplement.

Acknowledgements. Financial and logistical support for SOAS was provided by the NSF, the Earth Observing Laboratory at the National Center for Atmospheric Research (operated by NSF), the personnel at Atmospheric Research and Analysis, and the Electric Power Research Institute. We are grateful to Kevin Olson and Li Zhang for assistance with measurements during SOAS. Funding for the SEARCH network was provided by Southern Company Services and the Electric Power Research Institute. The Berkeley authors acknowledge the support of the NOAA Office of Global Programs grant NA13OAR4310067 and NSF grant AGS-1352972.

Edited by: Andreas Hofzumahaus
Reviewed by: two anonymous referees

References

Atkinson, R., Baulch, D. L., Cox, R. A., Crowley, J. N., Hampson, R. F., Hynes, R. G., Jenkin, M. E., Rossi, M. J., Troe, J., and IUPAC Subcommittee: Evaluated kinetic and photochemical data for atmospheric chemistry: Volume II – gas phase reactions of organic species, Atmos. Chem. Phys., 6, 3625–4055, https://doi.org/10.5194/acp-6-3625-2006, 2006.

Atkinson, R. W., Yu, D., Armstrong, B. G., Pattenden, S., Wilkinson, P., Doherty, R. M., Heal, M. R., and Anderson, H. R.: Concentration–Response Function for Ozone and Daily Mortality: Results from Five Urban and Five Rural U.K. Populations, Environ. Health Persp., 120, 1411–1417, 2012.

Ayres, B. R., Allen, H. M., Draper, D. C., Brown, S. S., Wild, R. J., Jimenez, J. L., Day, D. A., Campuzano-Jost, P., Hu, W., de Gouw, J., Koss, A., Cohen, R. C., Duffey, K. C., Romer, P., Baumann, K., Edgerton, E., Takahama, S., Thornton, J. A., Lee, B. H., Lopez-Hilfiker, F. D., Mohr, C., Wennberg, P. O., Nguyen, T. B., Teng, A., Goldstein, A. H., Olson, K., and Fry, J. L.: Organic nitrate aerosol formation via NO_3 + biogenic volatile organic compounds in the southeastern United States, Atmos. Chem. Phys., 15, 13377–13392, https://doi.org/10.5194/acp-15-13377-2015, 2015.

Barnes, E. A. and Fiore, A. M.: Surface ozone variability and the jet position: Implications for projecting future air quality, Geophys. Res. Lett., 40, 2839–2844, https://doi.org/10.1002/grl.50411, 2013.

Baumann, K., Williams, E. J., Angevine, W. M., Roberts, J. M., Norton, R. B., Frost, G. J., Fehsenfeld, F. C., Springston, S. R., Bertman, S. B., and Hartsell, B.: Ozone production and transport near Nashville, Tennessee: Results from the 1994 study at New Hendersonville, J. Geophys. Res., 105, 9137–9153, https://doi.org/10.1029/1999JD901017, 2000.

Berlin, S. R., Langford, A. O., Estes, M., Dong, M., and Parrish, D. D.: Magnitude, Decadal Changes, and Impact of Regional Background Ozone Transported into the Greater Houston, Texas, Area, Environ. Sci. Technol., 47, 13985–13992, https://doi.org/10.1021/es4037644, 2013.

Booker, F., Muntifering, R., McGrath, M., Burkey, K., Decoteau, D., Fiscus, E., Manning, W., Krupa, S., Chappelka, A., and Grantz, D.: The Ozone Component of Global Change: Potential Effects on Agricultural and Horticultural Plant Yield, Product Quality and Interactions with Invasive Species, J. Integr. Plant Biol., 51, 337–351, https://doi.org/10.1111/j.1744-7909.2008.00805.x, 2009.

Browne, E. C., Min, K.-E., Wooldridge, P. J., Apel, E., Blake, D. R., Brune, W. H., Cantrell, C. A., Cubison, M. J., Diskin, G. S., Jimenez, J. L., Weinheimer, A. J., Wennberg, P. O., Wisthaler, A., and Cohen, R. C.: Observations of total $RONO_2$ over the boreal forest: NO_x sinks and HNO_3 sources, Atmos. Chem. Phys., 13, 4543–4562, https://doi.org/10.5194/acp-13-4543-2013, 2013.

Cooper, O. R., Gao, R.-S., Tarasick, D., Leblanc, T., and Sweeney, C.: Long-term ozone trends at rural ozone monitoring sites across the United States, 1990–2010, J. Geophys. Res. Atmos., 117, D22307, https://doi.org/10.1029/2012JD018261, 2012.

Cooper, O. R., Parrish, D. D., Ziemke, J., Balashov, N. V., Cupeiro, M., Galbally, I. E., Gilge, S., Horowitz, L., Jensen, N. R., Lamarque, J.-F., Naik, V., Oltmans, S. J., Schwab, J., Shindell, D. T., Thompson, A. M., Thouret, V., Wang, Y., and Zbinden, R. M.: Global distribution and trends of tropospheric ozone: An observation-based review, Elem. Sci. Anth., 2, 000029, https://doi.org/10.12952/journal.elementa.000029, 2014.

Davidson, E. A., Potter, C. S., Schlesinger, P., and Klooster, S. A.: Model estimates of regional nitric oxide emissions from soils of the Southeastern United States, Ecol. Appl., 8, 748–759, https://doi.org/10.1890/1051-0761(1998)008[0748:MEORNO]2.0.CO;2, 1998.

Day, D. A., Wooldridge, P. J., Dillon, M. B., Thornton, J. A., and Cohen, R. C.: A thermal dissociation laser-induced fluorescence instrument for in situ detection of NO_2, peroxy nitrates, alkyl nitrates, and HNO_3, J. Geophys. Res., 107, 4046, https://doi.org/10.1029/2001JD000779, 2002.

Durre, I. and Yin, X.: Enhanced radiosonde data for studies of vertical structure, B. Am. Meteorol. Soc., 89, 1257–1262, https://doi.org/10.1175/2008BAMS2603.1, 2008.

Faloona, I. C., Tan, D., Lesher, R. L., Hazen, N. L., Frame, C. L., Simpas, J. B., Harder, H., Martinez, M., Di Carlo, P., Ren, X., and Brune, W. H.: A Laser-induced Fluorescence Instrument for Detecting Tropospheric OH and HO_2: Characteristics and Calibration, J. Atmos. Chem., 47, 139–167, https://doi.org/10.1023/B:JOCH.0000021036.53185.0e, 2004.

Farmer, D. K., Perring, A. E., Wooldridge, P. J., Blake, D. R., Baker, A., Meinardi, S., Huey, L. G., Tanner, D., Vargas, O., and Cohen, R. C.: Impact of organic nitrates on urban ozone production, Atmos. Chem. Phys., 11, 4085–4094, https://doi.org/10.5194/acp-11-4085-2011, 2011.

Feiner, P. A., Brune, W. H., Miller, D. O., Zhang, L., Cohen, R. C., Romer, P. S., Goldstein, A. H., Keutsch, F. N., Skog, K. M., Wennberg, P. O., Nguyen, T. B., Teng, A. P., DeGouw, J., Koss, A., Wild, R. J., Brown, S. S., Guenther, A., Edgerton, E., Baumann, K., and Fry, J. L.: Testing Atmospheric Oxidation in an Alabama Forest, J. Atmos. Sci., 73, 4699–4710, https://doi.org/10.1175/JAS-D-16-0044.1, 2016.

Frost, G. J., Trainer, M., Allwine, G., Buhr, M. P., Calvert, J. G., Cantrell, C. A., Fehsenfeld, F. C., Goldan, P. D., Herwehe, J., Hübler, G., Kuster, W. C., Martin, R., McMillen, R. T., Montzka, S. A., Norton, R. B., Parrish, D. D., Ridley, B. A., Shetter, R. E., Walega, J. G., Watkins, B. A., Westberg, H. H., and Williams, E. J.: Photochemical ozone production in the rural southeastern United States during the 1990 Rural Oxidants in the Southern Environment (ROSE) program, J. Geophys. Res., 103, 22491–22508, https://doi.org/10.1029/98JD00881, 1998.

Fu, T.-M., Zheng, Y., Paulot, F., Mao, J., and Yantosca, R. M.: Positive but variable sensitivity of August surface ozone to large-scale warming in the southeast United States, Nat. Clim. Change, 5, 454–458, https://doi.org/10.1038/nclimate2567, 2015.

Gilman, J. B., Burkhart, J. F., Lerner, B. M., Williams, E. J., Kuster, W. C., Goldan, P. D., Murphy, P. C., Warneke, C., Fowler, C., Montzka, S. A., Miller, B. R., Miller, L., Oltmans, S. J., Ryerson, T. B., Cooper, O. R., Stohl, A., and de Gouw, J. A.: Ozone variability and halogen oxidation within the Arctic and sub-Arctic springtime boundary layer, Atmos. Chem. Phys., 10, 10223–10236, https://doi.org/10.5194/acp-10-10223-2010, 2010.

Hansen, D. A., Edgerton, E. S., Hartsell, B. E., Jansen, J. J., Kandasamy, N., Hidy, G. M., and Blanchard, C. L.: The Southeastern Aerosol Research and Characterization Study: Part 1 – Overview, J. Air Waste Manage., 53, 1460–1471, https://doi.org/10.1080/10473289.2003.10466318, 2003.

Heagle, A. S.: Ozone and Crop Yield, Annu. Rev. Phytopathol., 27, 397–423, https://doi.org/10.1146/annurev.py.27.090189.002145, 1989.

Hickman, J. E., Wu, S., Mickley, L. J., and Lerdau, M. T.: Kudzu (*Pueraria montana*) invasion doubles emissions of nitric oxide and increases ozone pollution, Proc. Natl. Acad. Sci. USA, 107, 10115–10119, https://doi.org/10.1073/pnas.0912279107, 2010.

Hidy, G. M., Blanchard, C. L., Baumann, K., Edgerton, E., Tanenbaum, S., Shaw, S., Knipping, E., Tombach, I., Jansen, J., and Walters, J.: Chemical climatology of the southeastern United States, 1999–2013, Atmos. Chem. Phys., 14, 11893–11914, https://doi.org/10.5194/acp-14-11893-2014, 2014.

Hirsch, A. I., Munger, J. W., Jacob, D. J., Horowitz, L. W., and Goldstein, A. H.: Seasonal variation of the ozone production efficiency per unit NO_x at Harvard Forest, Massachusetts, J. Geophys. Res., 101, 12659–12666, https://doi.org/10.1029/96JD00557, 1996.

Hu, K. S., Darer, A. I., and Elrod, M. J.: Thermodynamics and kinetics of the hydrolysis of atmospherically relevant organonitrates and organosulfates, Atmos. Chem. Phys., 11, 8307–8320, https://doi.org/10.5194/acp-11-8307-2011, 2011.

Ito, K., De Leon, S. F., and Lippmann, M.: Associations Between Ozone and Daily Mortality: Analysis and Meta-Analysis, Epidemiology, 16, 446–457, https://doi.org/10.1097/01.ede.0000165821.90114.7f, 2005.

Jacob, D. J. and Winner, D. A.: Effect of climate change on air quality, Atmos. Environ., 43, 51–63, https://doi.org/10.1016/j.atmosenv.2008.09.051, 2009.

Jacob, D. J., Logan, J. A., Gardner, G. M., Yevich, R. M., Spivakovsky, C. M., Wofsy, S. C., Sillman, S., and Prather, M. J.: Factors regulating ozone over the United States and its export to the global atmosphere, J. Geophys. Res., 98, 14817–14826, https://doi.org/10.1029/98JD01224, 1993.

Jenkin, M. E., Young, J. C., and Rickard, A. R.: The MCM v3.3.1 degradation scheme for isoprene, Atmos. Chem. Phys., 15, 11433–11459, https://doi.org/10.5194/acp-15-11433-2015, 2015.

Kaser, L., Karl, T., Schnitzhofer, R., Graus, M., Herdlinger-Blatt, I. S., DiGangi, J. P., Sive, B., Turnipseed, A., Hornbrook, R. S., Zheng, W., Flocke, F. M., Guenther, A., Keutsch, F. N., Apel, E., and Hansel, A.: Comparison of different real time VOC measurement techniques in a ponderosa pine forest, Atmos. Chem. Phys., 13, 2893–2906, https://doi.org/10.5194/acp-13-2893-2013, 2013.

Kesik, M., Brüggemann, N., Forkel, R., Kiese, R., Knoche, R., Li, C., Seufert, G., Simpson, D., and Butterbach-Bahl, K.: Future scenarios of N_2O and NO emissions from European forest soils, J. Geophys. Res., 111, G02018, https://doi.org/10.1029/2005JG000115, 2006.

LaFranchi, B. W., Wolfe, G. M., Thornton, J. A., Harrold, S. A., Browne, E. C., Min, K. E., Wooldridge, P. J., Gilman, J. B., Kuster, W. C., Goldan, P. D., de Gouw, J. A., McKay, M., Goldstein, A. H., Ren, X., Mao, J., and Cohen, R. C.: Closing the peroxy acetyl nitrate budget: observations of acyl peroxy nitrates (PAN, PPN, and MPAN) during BEARPEX 2007, Atmos. Chem. Phys., 9, 7623–7641, https://doi.org/10.5194/acp-9-7623-2009, 2009.

Liu, S. and Liang, X.-Z.: Observed Diurnal Cycle Climatology of Planetary Boundary Layer Height, J. Climate, 23, 5790–5809, https://doi.org/10.1175/2010JCLI3552.1, 2010.

Mao, J., Ren, X., Brune, W. H., Olson, J. R., Crawford, J. H., Fried, A., Huey, L. G., Cohen, R. C., Heikes, B., Singh, H. B., Blake, D. R., Sachse, G. W., Diskin, G. S., Hall, S. R., and Shetter, R. E.: Airborne measurement of OH reactivity during INTEX-B, Atmos. Chem. Phys., 9, 163–173, https://doi.org/10.5194/acp-9-163-2009, 2009.

Mickley, L. J., Jacob, D. J., and Rind, D.: Uncertainty in preindustrial abundance of tropospheric ozone: Implications for radiative forcing calculations, J. Geophys. Res., 106, 3389–3399, https://doi.org/10.1029/2000JD900594, 2001.

Min, K.-E., Pusede, S. E., Browne, E. C., LaFranchi, B. W., and Cohen, R. C.: Eddy covariance fluxes and vertical concentration gradient measurements of NO and NO_2 over a ponderosa pine ecosystem: observational evidence for within-canopy chemical removal of NO_x, Atmos. Chem. Phys., 14, 5495–5512, https://doi.org/10.5194/acp-14-5495-2014, 2014.

Myhre, G. D., Shindell, D. T., Bréon, F.-M., Collins, W., Fuglestvedt, J., Huang, J., Koch, D., Lamarque, J.-F., Lee, D., Mendoza, B., Nakajima, T., Robock, A., Stephens, G., Takemura, T., and Zhang, H.: Anthropogenic and natural radiative forcing, in: Climate Change 2013: The Physical Science Basis. Contribution of Working Group I to the Fifth Assessment Report of the Intergovernmental Panel on Climate Change, edited by: Stocker, T. F., Qin, D., Plattner, G.-K., Tignor, M., Allen, S. K., Boschung, J., Nauels, A., Xia, Y., Bex, V., and Midgley, P. M., 659–740, Cambridge University Press, Cambridge, UK, 2013.

Oikawa, P. Y., Ge, C., Wang, J., Eberwein, J. R., Liang, L. L., Allsman, L. A., Grantz, D. A., and Jenerette, G. D.: Unusually high soil nitrogen oxide emissions influence air quality in a high-temperature agricultural region, Nat. Commun., 6, 8753, https://doi.org/10.1038/ncomms9753, 2015.

Oswald, R., Behrendt, T., Ermel, M., Wu, D., Su, H., Cheng, Y., Breuninger, C., Moravek, A., Mougin, E., Delon, C., Loubet, B., Pommerening-Röser, A., Sörgel, M., Pöschl, U., Hoffmann, T., Andreae, M. O., Meixner, F. X., and Trebs, I.: HONO Emissions from Soil Bacteria as a Major Source of Atmospheric Reactive Nitrogen, Science, 341, 1233–1235, https://doi.org/10.1126/science.1242266, 2013.

Peeters, J., Müller, J.-F., Stavrakou, T., and Nguyen, V. S.: Hydroxyl Radical Recycling in Isoprene Oxidation Driven by Hydrogen Bonding and Hydrogen Tunneling: The Upgraded LIM1 Mechanism, J. Phys. Chem. A, 118, 8625–8643, https://doi.org/10.1021/jp5033146, 2014.

Perring, A. E., Pusede, S. E., and Cohen, R. C.: An Observational Perspective on the Atmospheric Impacts of Alkyl and Multifunctional Nitrates on Ozone and Secondary Organic Aerosol, Chem. Rev., 113, 5848–5870, https://doi.org/10.1021/cr300520x, 2013.

Pilegaard, K.: Processes regulating nitric oxide emissions from soils, Philos. T. Roy. Soc. B, 368, 20130126, https://doi.org/10.1098/rstb.2013.0126, 2013.

Pilegaard, K., Skiba, U., Ambus, P., Beier, C., Brüggemann, N., Butterbach-Bahl, K., Dick, J., Dorsey, J., Duyzer, J., Gallagher, M., Gasche, R., Horvath, L., Kitzler, B., Leip, A., Pihlatie, M. K., Rosenkranz, P., Seufert, G., Vesala, T., Westrate, H., and Zechmeister-Boltenstern, S.: Factors controlling regional differences in forest soil emission of nitrogen oxides (NO and N_2O), Biogeosciences, 3, 651–661, https://doi.org/10.5194/bg-3-651-2006, 2006.

Pleijel, H., Danielsson, H., Ojanperä, K., De Temmerman, L., Högy, P., Badiani, M., and Karlsson, P. E.: Relationships between ozone exposure and yield loss in European wheat and potato—a comparison of concentration- and flux-based exposure indices, Atmos. Environ., 38, 2259–2269, https://doi.org/10.1016/j.atmosenv.2003.09.076, 2004.

Pusede, S. E., Gentner, D. R., Wooldridge, P. J., Browne, E. C., Rollins, A. W., Min, K.-E., Russell, A. R., Thomas, J., Zhang, L., Brune, W. H., Henry, S. B., DiGangi, J. P., Keutsch, F. N., Harrold, S. A., Thornton, J. A., Beaver, M. R., St. Clair, J. M., Wennberg, P. O., Sanders, J., Ren, X., VandenBoer, T. C., Markovic, M. Z., Guha, A., Weber, R., Goldstein, A. H., and Cohen, R. C.: On the temperature dependence of organic reactivity, nitrogen oxides, ozone production, and the impact of emission controls in San Joaquin Valley, California, Atmos. Chem. Phys., 14, 3373–3395, https://doi.org/10.5194/acp-14-3373-2014, 2014.

Pusede, S. E., Steiner, A. L., and Cohen, R. C.: Temperature and Recent Trends in the Chemistry of Continental Surface Ozone, Chem. Rev., 115, 3898–3918, https://doi.org/10.1021/cr5006815, 2015.

Romer, P. S., Duffey, K. C., Wooldridge, P. J., Allen, H. M., Ayres, B. R., Brown, S. S., Brune, W. H., Crounse, J. D., de Gouw, J., Draper, D. C., Feiner, P. A., Fry, J. L., Goldstein, A. H., Koss, A., Misztal, P. K., Nguyen, T. B., Olson, K., Teng, A. P., Wennberg, P. O., Wild, R. J., Zhang, L., and Cohen, R. C.: The lifetime of nitrogen oxides in an isoprene-dominated forest, Atmos. Chem. Phys., 16, 7623–7637, https://doi.org/10.5194/acp-16-7623-2016, 2016.

Ryerson, T. B., Williams, E. J., and Fehsenfeld, F. C.: An efficient photolysis system for fast-response NO_2 measurements, J. Geophys. Res. Atmos., 105, 26447–26461, https://doi.org/10.1029/2000JD900389, 2000.

Shen, L., Mickley, L. J., and Gilleland, E.: Impact of increasing heat waves on U.S. ozone episodes in the 2050s: Results from a multimodel analysis using extreme value theory, Geophys. Res. Lett., 43, 4017–4025, https://doi.org/10.1002/2016GL068432, 2016.

Sillman, S. and Samson, P. J.: Impact of temperature on oxidant photochemistry in urban, polluted rural and remote environments, J. Geophys. Res., 100, 11497–11508, https://doi.org/10.1029/94JD02146, 1995.

Singh, R. B. and Sloan, J. J.: A high-resolution NO_x emission factor model for North American motor vehicles, Atmos. Environ., 40, 5214–5223, https://doi.org/10.1016/j.atmosenv.2006.04.012, 2006.

SOAS Science Team: SOAS 2013 Centreville Site Data, NOAA, https://esrl.noaa.gov/csd/groups/csd7/measurements/2013senex/Ground/DataDownload (last access: 17 June 2017), 2013.

Steiner, A. L., Tonse, S., Cohen, R. C., Goldstein, A. H., and Harley, R. A.: Influence of future climate and emissions on regional air quality in California, J. Geophys. Res., 111, D18303, https://doi.org/10.1029/2005JD006935, 2006.

Steiner, A. L., Davis, A. J., Sillman, S., Owen, R. C., Michalak, A. M., and Fiore, A. M.: Observed suppression of ozone formation at extremely high temperatures due to chemical and biophysical feedbacks, Proc. Natl. Acad. Sci. USA, 107, 19685–19690, https://doi.org/10.1073/pnas.1008336107, 2010.

Thornton, F. C., Pier, P. A., and Valente, R. J.: NO emissions from soils in the southeastern United States, J. Geophys. Res., 102, 21189–21195, https://doi.org/10.1029/97JD01567, 1997.

Trainer, M., Parrish, D. D., Buhr, M. P., Norton, R. B., Fehsenfeld, F. C., Anlauf, K. G., Bottenheim, J. W., Tang, Y. Z., Wiebe, H. A., Roberts, J. M., Tanner, R. L., Newman, L., Bowersox, V. C., Meagher, J. F., Olszyna, K. J., Rodgers, M. O., Wang, T., Berresheim, H., Demerjian, K. L., and Roychowdhury, U. K.: Correlation of ozone with NO_y in photochemically aged air, J. Geophys. Res., 98, 2917–2925, https://doi.org/10.1029/92JD01910, 1993.

Travis, K. R., Jacob, D. J., Fisher, J. A., Kim, P. S., Marais, E. A., Zhu, L., Yu, K., Miller, C. C., Yantosca, R. M., Sulprizio, M. P., Thompson, A. M., Wennberg, P. O., Crounse, J. D., St. Clair, J. M., Cohen, R. C., Laughner, J. L., Dibb, J. E., Hall, S. R., Ullmann, K., Wolfe, G. M., Pollack, I. B., Peischl, J., Neuman, J. A., and Zhou, X.: Why do models overestimate surface ozone in the Southeast United States?, Atmos. Chem. Phys., 16, 13561–13577, https://doi.org/10.5194/acp-16-13561-2016, 2016.

Trebs, I., Bohn, B., Ammann, C., Rummel, U., Blumthaler, M., Königstedt, R., Meixner, F. X., Fan, S., and Andreae, M. O.: Relationship between the NO_2 photolysis frequency and the solar global irradiance, Atmos. Meas. Tech., 2, 725–739, https://doi.org/10.5194/amt-2-725-2009, 2009.

VandenBoer, T. C., Brown, S. S., Murphy, J. G., Keene, W. C., Young, C. J., Pszenny, A. A. P., Kim, S., Warneke, C., de Gouw, J. A., Maben, J. R., Wagner, N. L., Riedel, T. P., Thornton, J. A., Wolfe, D. E., Dubé, W. P., Öztürk, F., Brock, C. A., Grossberg, N., Lefer, B., Lerner, B., Middlebrook, A. M., and Roberts, J. M.: Understanding the role of the ground surface in HONO vertical structure: High resolution vertical profiles during NACHTT-11, J. Geophys. Res. Atmos., 118, 10155–10171, https://doi.org/10.1002/jgrd.50721, 2013.

Vedal, S., Brauer, M., White, R., and Petkau, J.: Air Pollution and Daily Mortality in a City with Low Levels of Pollution, Environ. Health Persp., 111, 45–51, https://doi.org/10.14288/1.0220733, 2003.

Weaver, C. P., Liang, X.-Z., Zhu, J., Adams, P. J., Amar, P., Avise, J., Caughey, M., Chen, J., Cohen, R. C., Cooter, E., Dawson, J. P., Gilliam, R., Gilliland, A., Goldstein, A. H., Grambsch, A., Grano, D., Guenther, A., Gustafson, W. I., Harley, R. A., He, S., Hemming, B., Hogrefe, C., Huang, H.-C., Hunt, S. W., Jacob, D., Kinney, P. L., Kunkel, K., Lamarque, J.-F., Lamb, B., Larkin, N. K., Leung, L. R., Liao, K.-J., Lin, J.-T., Lynn, B. H., Manomaiphiboon, K., Mass, C., McKenzie, D., Mickley, L. J., O'Neill, S. M., Nolte, C., Pandis, S. N., Racherla, P. N., Rosenzweig, C., Russell, A. G., Salathé, E., Steiner, A. L., Tagaris, E., Tao, Z., Tonse, S., Wiedinmyer, C., Williams, A., Winner, D. A., Woo, J.-H., Wu, S., and Wuebbles, D. J.: A Preliminary Synthesis of Modeled Climate Change Impacts on U.S. Regional Ozone Concentrations, B. Am. Meteorol. Soc., 90, 1843–1863, https://doi.org/10.1175/2009BAMS2568.1, 2009.

Williams, E. J. and Fehsenfeld, F. C.: Measurement of soil nitrogen oxide emissions at three North American ecosystems, J. Geophys. Res., 96, 1033–1042, https://doi.org/10.1029/90JD01903, 1991.

Wolfe, G. M., Marvin, M. R., Roberts, S. J., Travis, K. R., and Liao, J.: The Framework for 0-D Atmospheric Modeling (F0AM) v3.1, Geosci. Model Dev., 9, 3309–3319, https://doi.org/10.5194/gmd-9-3309-2016, 2016.

World Health Organization: Air Quality Guidelines: Global Update 2005, Particulate Matter, Ozone, Nitrogen Dioxide and Sulphur Dioxide, WHO Regional Office for Europe, Copenhagen, Denmark, 2005.